Available online at www.sciencedirect.com
SCIENCE DIRECT®
Journal of Solid State Chemistry 177 (2004) 4119–4125
JOURNAL OF SOLID STATE CHEMISTRY
www.elsevier.com/locate/jssc

Effect of pH on the formation and combustion process of sol–gel auto-combustion derived NiZn ferrite/SiO_2 composites

K.H. Wu[a,*], C.H. Yu[a], Y.C. Chang[b], D.N. Horng[b]

[a]*Department of Applied Chemistry, Chung Cheng Institute of Technology, NDU, Tahsi, Taoyuan 335, Taiwan, ROC*
[b]*Department of Chemistry, Chinese Military Academy, Fengshan, Kaohsiung 830, Taiwan, ROC*

Received 15 June 2004; received in revised form 27 July 2004; accepted 31 July 2004
Available online 7 October 2004

Abstract

A nitrate–citrate–silica gel was prepared from metallic nitrates, citric acid, and silica powder by sol–gel process, and it was further used to synthesize $Ni_{0.5}Zn_{0.5}Fe_2O_4$/5wt% SiO_2 nanocomposites by auto-combustion. The effect of pH on the formation of NiZn ferrite/SiO_2 and thermal properties of gel precursors was studied by XRD, IR, EPR, TGA and DTA techniques. The results revealed that the ratio of the citrate ion to the nitrate ion is directly related to the pH of the solution. The pH in the starting solution affects the combustion process, and then determines the particle size of the as-synthesized powder. The EPR parameters (peak-to-peak linewidth, g factor, and spin number) increased with increasing pH, whereas the spin–spin relaxation time (T_2) decreased. The thermal stability and enthalpy of the decomposition process in air decreased with increasing pH, whereas the enthalpy in nitrogen increased. Moreover, the activation energy (E_a) of thermo-oxidative degradation of the gel precursor at pH 3 was much lower than the gel precursor at pH 5 and 7, and that increased with increasing pH.

Keywords: Sol–gel; Auto-combustion; NiZn ferrite; Activation energy; EPR

1. Introduction

Magnetic properties of crystalline materials dispersed in a non-magnetic matrix, either porous or not, have been studied in ferrite/SiO_2 [1–3], ferrite/resin [4–6], ferrite/polymer [7,8], and ferrite/forsterite system [9]. These types of composite, if formed from nanoparticles, enhance their magnetic properties as compared with the magnetic materials obtained by conventional processes [10,11]. These composites also have other interesting properties such as catalytic activity, structural stability, and electrical resistance, depending on the kind and the concentration of the component used and their structural characteristics [10,11].

Many synthetic approaches have been employed to prepare magnetic nanocrystals [12–16]. The nanocrystals obtained usually have a strong tendency to aggregate, which makes it very difficult to exploit their unique physical properties. Dispersion of the nanocrystals in a matrix is one method for reducing particle agglomeration [17] and this technique allows one to stabilize the particles and to study their formation reactions [13]. The sol–gel auto-combustion technique is a novel way with a unique combination of the chemical sol–gel process and the combustion process. The synthesis has been used to create different ceramic systems [18–20]. Yue et al. [20] have reported the effect of molar ratio of metal nitrates to citric acid on the combustion process of NiCuZn ferrite. According to their study, the combustion rate can be controlled by changing the ratio of nitrates to citric acid in starting solutions. Thus, the particle size of NiCuZn ferrite powder depends on the ratio of metal nitrates to citric acid. Similar studies of varying acid to metal ion ratios were performed for citric acid-assisted synthesis of $LiNi_{0.8}Co_{0.2}O_2$ [21], which resulted in

*Corresponding author. Fax: +886-3-389-1519.
E-mail address: khwu@ccit.edu.tw (K.H. Wu).

0022-4596/$ - see front matter © 2004 Elsevier Inc. All rights reserved.
doi:10.1016/j.jssc.2004.07.056

decreased in capacity values with higher acid to metal ion ratios. However, the thermodynamic and spin dynamic performance of the materials synthesized with varying pH have not been reported.

Electron paramagnetic resonance (EPR) is a powerful tool in investigation of internal fields and spin dynamics in solids. More detailed information on magnetic and electronic state can be extracted from the measurements of electron spin relaxation. Thermal analysis plays an important role in the determination and identification of materials, change in phase, thermal dehydration and decomposition reactions, solid-state formation, and kinetic studies. In our previous paper [22], a series of $(Ni_{0.5}Zn_{0.5}Fe_2O_4)_{100-x}(SiO_2)_x$ ($x = 5$, 10, 20 wt%) nanocomposites were prepared using sol–gel auto-combustion method, and we found that the nitrate–citrate–silica gels exhibited self-propagating combustion behavior and it directly transformed into nanosized (8–16 nm) NiZn ferrite particles with spinel crystal structure after combustion. The content of silica in the starting solution affects the combustion process, enhances interaction between the NiZn ferrite and silica, and reduces NiZn ferrite agglomeration. In the present paper we investigate the effect of pH on the formation and combustion processes of NiZn ferrite doped with silica powder using sol–gel auto-combustion method. The results are greatly affecting the structure, thermal, and spin dynamic properties. Varying pH and its effect on the enthalpy, apparent activation energy of the decomposition process of the gel precursors, particle size, and EPR characteristics of $Ni_{0.5}Zn_{0.5}Fe_2O_4$/5wt% SiO_2 are described in detail.

2. Experimental

2.1. Preparation of NiZn ferrite/SiO_2 nanocomposite

Analytical grade nickel nitrate, zinc nitrate, iron nitrate, citric acid, and silica powder were used as raw materials to prepare $Ni_{0.5}Zn_{0.5}Fe_2O_4$/5 wt% SiO_2 nanocomposite. The initial molar ratio was Ni:Zn:Fe = 1:1:4. First, 2.0 g $Ni(NO_3)_2 \cdot 6H_2O$, 2.05 g $Zn(NO_3)_2 \cdot 6H_2O$, and 11.12 g $Fe(NO_3)_3 \cdot 9H_2O$ were dissolved in 60 mL of deionized water, and then 5 wt% of SiO_2 powder (Aerosil 200; <100 nm) was added into the solution. The molar ratio of nitrates to citric acid was 1:1. A small amount of ammonia was added to the solution to adjust the pH value to about 3, 5, and 7. The entire mixture was thoroughly stirred for 6 h at 70 °C. Then, the mixed solution was poured into a Teflon dish and heated 24 h at 60 °C and 3 h at 100 °C under a vacuum to obtain a dried gel. When ignited at any point, the dried gel burnt in a self-propagating combustion manner until all the gels were burnt out completely to form a loose powder. A schematic diagram of the preparation process is shown in Fig. 1.

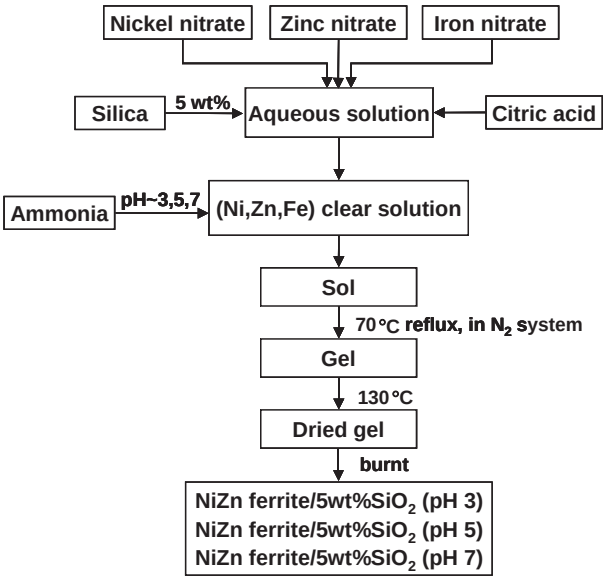

Fig. 1. Schematic diagram of the preparation of $Ni_{0.5}Zn_{0.5}Fe_2O_4/SiO_2$ powder.

2.2. Characterization of NiZn ferrite/SiO_2 nanocomposite

The phase identification of the as-burnt powder was performed using X-ray diffraction (XRD; SIEMENS D5000) with CuK_α radiation. Average grain sizes (D) were determined from the XRD peaks using Scherrer's formula. Infrared spectra (IR) of the gel precursor and the as-burnt powder were recorded on a Bomem DA 3.002 spectrophotometer from 400 to 4000 cm^{-1} by the KBr pellet method. The EPR spectra were recorded at room temperature with a Bruker EMX-10 spectrometer operating in the X-band ($\mu = 9.6$ GHz) with 100 kHz field modulation. DPPH ($g = 2.0036$) was used as a field marker. The characteristics and kinetics of decomposition of the gel precursors were examined by a Perkin-Elmer TGA-2 at heating rate of 10 °C/min under air and nitrogen. The sample weight was about 10 mg, and the gas flow rate was kept at 100 mL/min.

2.3. Kinetic analysis

The degree of conversion α is defined as the ratio of actual weight loss to total weight loss. Therefore, the rate of degradation $d\alpha/dt$, dependent on temperature and weight of sample, is given by

$$da/dt = k(T) \times f(a), \quad (1)$$

where $k(T)$ is the rate constant and $f(\alpha)$ is the conversion functional relationship. If $k(T) = A\exp(-E_a/RT)$ and $f(\alpha) = (1-\alpha)^n$, then Eq. (1) can be expressed as

$$da/dt = A\exp(-E_a/RT)(1-a)^n, \quad (2)$$

where A, E_a, R, T, and n represent pre-exponential factor, activation energy, gas constant, temperature, and reaction order, respectively. By integrating Eq. (2) and introducing the initial condition of $\alpha = 0$ at $T = T_0$ the following expression is obtained:

$$g(\alpha) = \int_0^{\alpha} \frac{d\alpha}{(1-\alpha)^n} = \frac{A}{q}\int_{T_0}^{T} \exp\left(\frac{-E_a}{RT}\right) dT, \quad (3)$$

where q is the heating rate (dT/dt). For the special case $n = 1$,

$$g(\alpha) = \int_0^{\alpha} \frac{d\alpha}{(1-\alpha)^n} = -\ln(1-\alpha). \quad (4)$$

For n not equal to zero or unit,

$$g(\alpha) = \int_0^{\alpha} \frac{d\alpha}{(1-\alpha)^n} = -\frac{1-(1-\alpha)^{1-n}}{1-n}. \quad (5)$$

The reaction order n of thermo-oxidative degradation in this paper was determined by Kissinger's equation [23]. Several techniques using different approaches were developed for solving the integral of Eq. (3). The method investigated in this work was that by van Krevelen [24].

Van Krevelen method for $n \neq 1$ gave the following expression:

$$\ln g(\alpha) = \ln\left[\frac{A(0.368/T_m)^x}{q(x+1)}\right] + (x+1)\ln T \quad (6)$$

$$\text{for } n = 1; \quad \ln g(\alpha) = (x+1)\ln T, \quad (7)$$

where $x = E_a/RT_m$. The activation energies were evaluated from the slopes in plot of $\ln g(\alpha)$ versus $\ln T$.

3. Results and discussion

3.1. Formation of gels and grain size

The pH of solution was regulated to control the rate of turning sols to gels and the diameter of the grains in this study. In solution-based synthesis, the formation of chelation complexes depends on the pH of the solution. The experimental results showed that the solution of mixed reactants was dark green and finally produced brown dried gel at pH 5 and 7. At pH 3, the citric acid can facilitate the gelation ability of the mixed solution and the solution was dark blue. Formation of a chelation complex is important in preventing the segregation or precipitation of transition metal ions [25].

Fig. 2 shows the X-ray diffraction (XRD) pattern of as-burnt powder with different pH values. The diffraction peaks are broadened with decrease of pH value, suggesting that the crystallite size of the ferrite decreases with decreasing pH value. The NiZn ferrite at pH 3 and 5 exhibits more X-ray peaks than ferrite at pH 7, which corresponds to the impurities of F_2O_3. Crystallite sizes

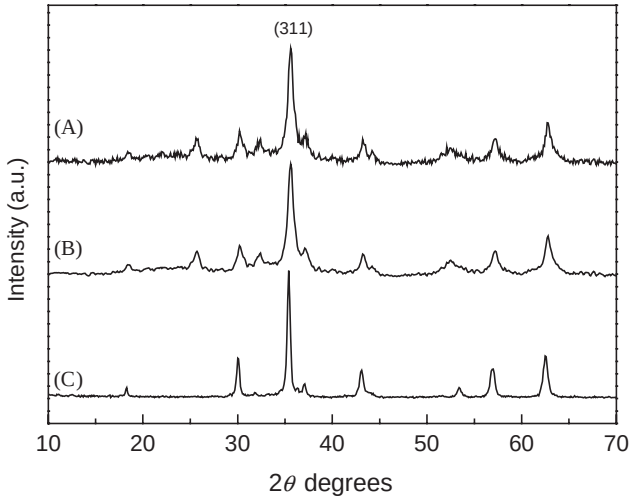

Fig. 2. XRD spectra of NiZn ferrite/5 wt% SiO_2 at (A) pH 3, (B) pH 5, (C) pH 7.

of the ferrite are calculated from the X-ray peak broadening of the (311) diffraction peak using Scherrer's formula [26]:

$$D = 0.9\,\lambda/\beta\cos\theta, \quad (8)$$

where D is the crystallite size in nm, λ the radiation wavelength (0.154 nm for CuK_α), β the bandwidths at half-height and θ the diffraction peak angle. The calculated crystallite sizes are 13, 16, and 25 nm, respectively, for NiZn ferrite/5 wt% SiO_2 at pH 3, 5, and 7. It was evident that the crystallite size of the ferrite phase depending on pH, which was fairly consistent with the particle size, was determined by transmission electron microscopy (Fig. 3). Solution-based synthesis methods are sensitive to pH, which determines the formation of the compound as well as its burning performance.

3.2. Infrared spectra

Fig. 4 shows the IR spectra of the dried nitrate–citrate–SiO_2 gels and as-burnt powder. All the dried gels show characteristic bands of nitrate–citrate precursors and silica. The bands at about 3150, 1615, and 1390 cm^{-1} correspond to the O–H group of citric acid, carboxyl group, and anti-symmetric NO_3^- stretching vibration, respectively. The silica network is characterized by the strong absorptions at 3450, 1100, 830, and 470 cm^{-1}, corresponding to the silanol groups (Si–OH), Si–O–Si anti-symmetric stretch, symmetric stretch, and bending mode. In the IR curves of the as-burnt powder, a new band appears at 590 cm^{-1}. That is the characteristic band of NiZn ferrite and Fe–O stretching in Fe–O–Si bonds [13]. On the other hand, the disappearance or decrease at 1615 and 1390 cm^{-1} of the as-burnt

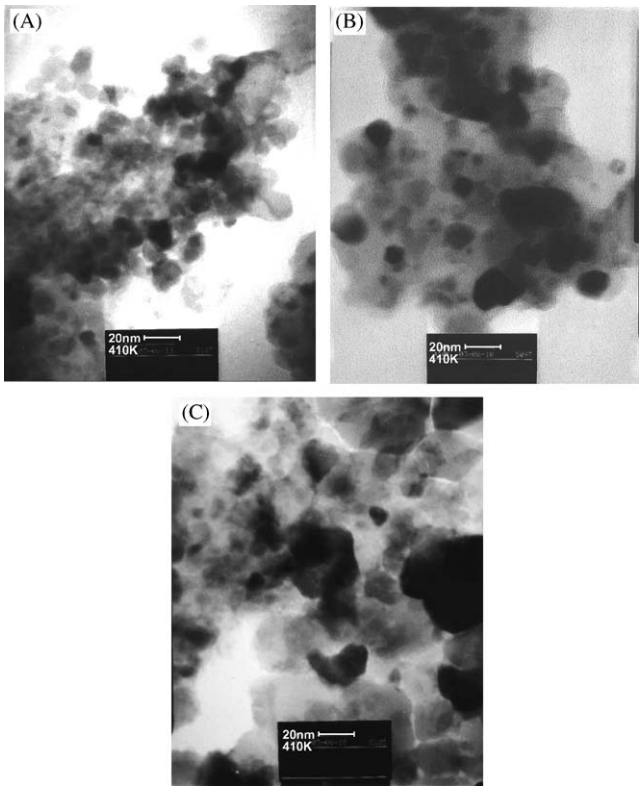

Fig. 3. TEM photograph of $Ni_{0.5}Zn_{0.5}Fe_2O_4/5wt\%SiO_2$ composites with different pH (A) pH 3, (B) pH 5 and (C) pH 7.

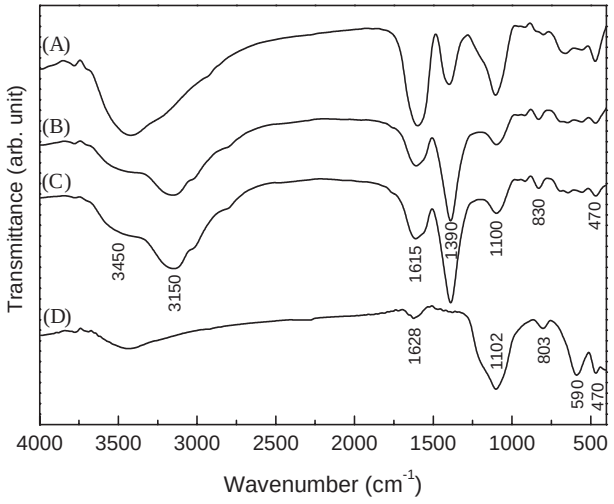

Fig. 4. IR spectra of (A) the dried gel at pH 3, (B) the dried gel at pH 5, (C) the dried gel at pH 7, (D) NiZn ferrite/5 wt% SiO_2 (pH 5).

powder (Fig. 4D) reveals that the carboxyl groups and the NO_3^- ions take part in the reaction during combustion.

Fig. 5 illustrates the effect of pH on the absorption intensities at 1100 cm^{-1} (Si–O–Si stretch), 1390 cm^{-1} (NO_3^- stretch), and 1615 cm^{-1} (carboxyl group stretch) for dried gel. In order to examine the result more

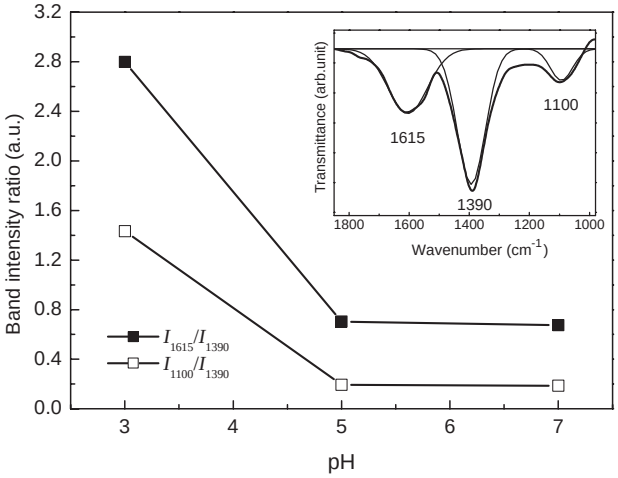

Fig. 5. The intensity ratio of I_{1615}/I_{1390} and I_{1100}/I_{1390} as a function of the pH value. The deconvoluted spectra of Fig. 3B between 1850 and 960 cm^{-1} are presented in the inset. Where I_{1100}, I_{1390} and I_{1615} are the areas of the peaks at 1100, 1390 and 1615 cm^{-1}, respectively, in the deconvoluted spectra.

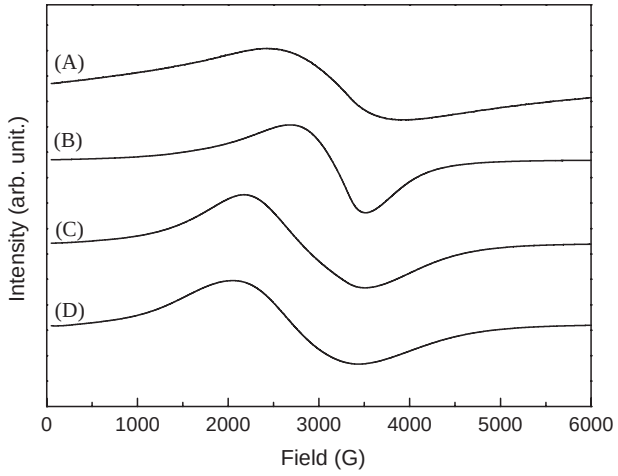

Fig. 6. EPR spectra of (A) the dried gel at pH 5, (B) NiZn ferrite/5wt% SiO_2 (pH 3), (C) NiZn ferrite/5wt% SiO_2 (pH 5), (D) NiZn ferrite/5 wt% SiO_2 (pH 7).

thoroughly, the peak areas at 1100, 1390, and 1615 cm^{-1} are fitted using Gaussian function. The intensity ratios of I_{1100}/I_{1390} and I_{1615}/I_{1390} as a function of the pH value are evaluated from the deconvoluted spectra (Fig. 5 inset), and the intensity ratio decreases with increasing pH. The result indicates that pH significantly affects the concentration ratio of Si–O–Si and citrate ion to nitrate ion.

3.3. Electron paramagnetic resonance spectra

The EPR spectra of dried gel and as-burnt powders have been recorded at room temperature, as shown in Fig. 6. It can be observed that the EPR spectra shows a single broad signal, indicating that the isolated Fe^{3+},

Table 1
EPR characteristics of NiZn ferrite/5 wt% SiO^2 composites with different pH values at room temperature[a]

Sample	D (nm)	ΔH_{PP} (G)	g factor	N_S ($\times 10^{10}$ spins/g)	T_2 ($\times 10^{-11}$ s)
Dried gel		1549	2.12	3.38	2.94
pH 3	13	833	2.20	1.20	5.39
pH 5	16	1351	2.44	3.15	2.92
pH 7	25	1385	2.52	3.34	2.77

[a] D is the crystallite size; ΔH_{PP}, the peak-to-peak linewidth; N_S, the spin number; T_2, the spin–spin relaxation time.

Ni^{2+}, and Zn^{2+} ions do not exist. Furthermore, we performed quantitative EPR measurements and the results are shown in Table 1. All the spectra were analyzed using Gaussian distribution function and the parameters like peak-to-peak linewidth (ΔH_{PP}), g factor, spin number (N_S), and spin–spin relaxation time (T_2) were obtained. As shown in Fig. 6A, a single resonance line at $g = 2.12$ was the combined contribution of the Fe^{3+}, Ni^{2+}, and Zn^{2+} ions, indicating that these transition metals appeared to participate directly in the sol–gel chemistry. When the gel was dried, these isolated transition metals are complexed with citric acid or probably distributed uniformly throughout the pores of the silica, and Fe^{3+} ions still have some weak interactions with the silica through Fe–O–Si bonds [13].

The EPR parameters (i.e., ΔH_{PP}, g factor and N_S) increase with increasing pH and particle size (Table 1). The results may be ascribed to the increased crystallization degree of $Ni_{0.5}Zn_{0.5}Fe_2O_4$ particles with increasing pH and particle size as revealed by XRD. This could make the spin number of Fe^{3+} increase and the interaction among the paramagnetic centers increase [27]. The spin relaxation process is characterized by a time constant, which is a function of static magnetic field and depends on the rate at which microwave energy can be absorbed and dissipated. The spin–spin relaxation process is the energy difference (ΔE), the energy absorbed from the radio-frequency source, transferred to neighboring electrons and the relaxation time (T_2) can be determined from peak-to-peak linewidth according to

$$\frac{1}{T_2} = \frac{g\beta\Delta H_{1/2}}{\hbar}, \quad \Delta H_{1/2} = \sqrt{3}\Delta H_{PP} \tag{9}$$

(in s^{-1}), where β is the Bohr magneton (9.274×10^{-21} erg/G), $\Delta H_{1/2}$ the linewidth (in G) at half-height of the absorption peak, and $\hbar$ a constant (1.054×10^{-27} erg s) [28]. The spin–spin relaxation time is correlated with the peak-to-peak linewidth of EPR. In this case T_2 decreases with increasing pH, indicating that the spin relaxation at pH 3 exhibits a slow relaxation (high T_2) and a fast relaxation (low T_2) at pH 5 and pH 7. The result may be due to the motion of composites being restricted by agglomeration at a higher pH value. It is interesting to note that magnetic ions in the $Ni_{0.5}Zn_{0.5}Fe_2O_4$/5 wt% SiO_2 composites with different pH can be found in different environments.

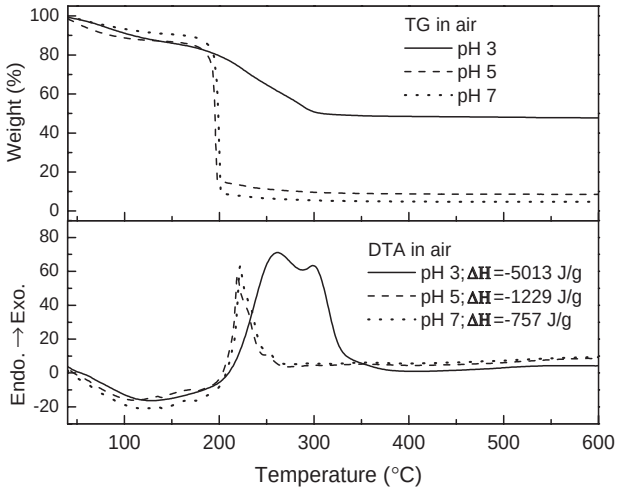

Fig. 7. TGA and DTA thermograms of the dried citrate–nitrate–5 wt% SiO_2 gel under air at the heating rate 10 °C/min.

3.4. Thermal analysis

The autocatalytic nature of the combustion process of nitrate–citrate–SiO_2 gel was studied by thermal analysis. Fig. 7 shows TG and DTA results for the dried gel precursors with different pH under air. The decomposition rate increases with increasing pH value, indicating that the decomposition rate is associated with the ratio of citrate ion to nitrate ion. The increase in pH would lead to an increase in NO_3^- ion content and increase in decomposition rate, because the nitrate ions provide an in situ oxidizing environment for the decomposition of the organic component [21]. Here, the variety in the pH results is a noticeable difference in the major decomposition reaction.

In the case of the gel precursor with pH 3, the initial weight loss which occurred in the temperature range 40–150 °C was mainly due to the dehydration, which is accompanied by an endothermic peak at about 120 °C in the DTA curve. The second stage of weight loss in the temperature range 150–270 °C was attributable to the decomposition of nitrates and citrate to carbonate. This process shows an exothermic peak at around 260 °C in

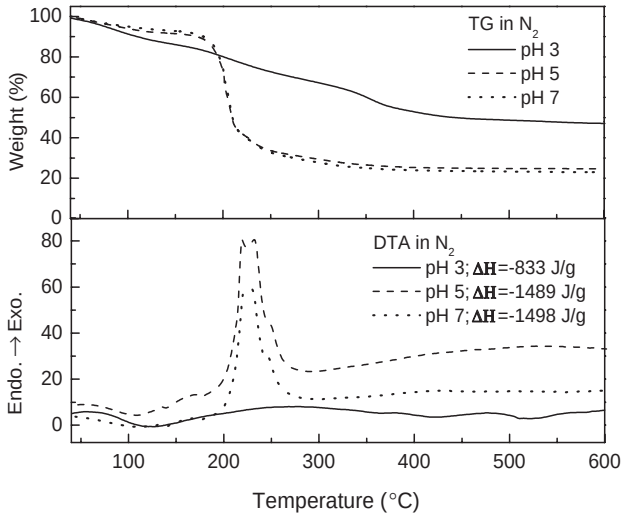

Fig. 8. TGA and DTA thermograms of the dried citrate–nitrate–5 wt% SiO_2 gel under nitrogen at the heating rate 10 °C/min.

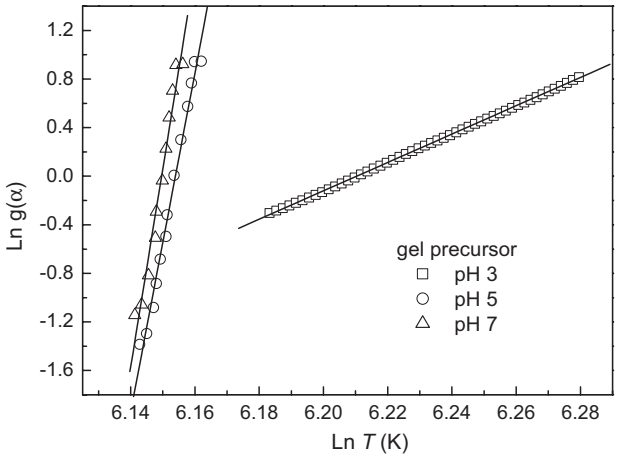

Fig. 9. Plot of $\ln g(\alpha)$ versus $\ln T$ for thermo-oxidative degradation of the dried citrate–nitrate–5 wt% SiO_2 gels.

the DTA curve. The final step in weight loss which occurred between 270 and 320 °C signified the decomposition of carbonate complex to NiZn ferrite, which is accompanied by an exothermic peak at around 300 °C in the DTA curve. Moreover, the weight loss of pH 3 was slower than that of pH 5 and 7, whereas the char yield (final weight residue) increases. This is due to the pyrolysis processes are very sluggish and gases are released out slowly [29]. On the other hand, a large exothermic peak ($\Delta H = -5013$ J/g) observed at pH 3 and the enthalpy (ΔH) decreases with increasing pH. This is attributed to the citrate–nitrate gel decomposition accompanied by the exothermic oxidation reaction, when the ratio between citric acid (fuel) and oxidizer (metal nitrates) increased.

Fig. 8 shows TG and DTA results for the dried gel precursors with different pH under nitrogen. In comparison with the spectra shown in Fig. 7, the thermal history of the gel precursors showed a similar step-like pattern of weight loss. However, the weight loss was slower than that in air and the enthalpy increases with increasing pH. The results may be due to the autocatalytic anionic oxidation–reduction reaction between the nitrate and citrate system being restrained in nitrogen and then the rate of the oxidation reaction relatively decreases. Moreover, at pH 5 and 7, about 70–90 wt% of the weight loss for the gel precursors occurred in air and nitrogen because a large amount of gases was released when the temperature of pyrolysis was 180 °C.

3.5. Kinetic analysis

The reaction order (n) of the thermo-oxidative degradation in the second stage, determined by Kissinger's equation, is dependent on pH. Fig. 9 shows the logarithmic plot for the degradation rate $g(\alpha)$ of the gel precursors versus temperature under air. The reaction order (n) and apparent activation energy (E_a), evaluated by van Krevelen method, are listed in Table 2. The E_a value of the thermo-oxidative degradation of the gel precursors at pH 3 is much lower than that gel precursor at pH 5 and 7, and that increases with increasing pH. The dramatic decrease of the E_a may be associated with the higher enthalpy of the gel precursor at pH 3, as is evident from the DTA curve shown in Fig. 7. The excessive heat transfer would allow ease rupture of the metal–oxygen bond in the gel precursor [30]. Rupture of the M–O bond would be followed by rupture of the C–O bond which would lead to the formation of the ferrite.

4. Conclusions

Variations in the structure, thermal, spin dynamic, and kinetic properties of the composites synthesized at different pH revealed that varying the citrate ion to nitrate ion ratio affected the formation/decomposition reaction, which was dependent on the pH of the solution. The ratio of citrate ion to nitrate ion can be observed from the band intensity of the gel precursor in the FTIR spectra. Increasing the pH resulted in increase in decomposition rate and particle size. The EPR characteristics for fine particles were presented and discussed in terms of the pH effect. The systematic increase in ESR parameters and decrease in T_2 observed in our present study were attributed to the increase of particle size with increasing pH value.

The E_a value of the thermo-oxidative degradation of the gel precursors at pH 3 (55 kJ/mol) was much lower than the gel precursor at pH 5 (536 kJ/mol) and pH 7 (633 kJ/mol), whereas the enthalpy of the gel precursors at pH 3 (−5013 J/g) was much more than the gel precursor at pH 5 (−1229 J/g) and pH 7 (−757 J/g). The

Table 2
Activation parameters[a] of the citrate–nitrate gel precursor thermo-oxidative degradation at heating rate of 10 °C/min under air

Samples	$T_{m\ (K)}$	n	E_a (kJ/mol)
NiZn ferrite/5 wt% SiO_2 (pH 3)	520	1.76	55
NiZn ferrite/5 wt% SiO_2 (pH 5)	469	1.01	536
NiZn ferrite/5 wt% SiO_2 (pH 7)	465	0.85	633

[a] T_m is the temperature at maximum rate of weight loss, n the reaction order, E_a the activation energy of the thermo-oxidative degradation.

consequences may be due to the citrate–nitrate gel decomposition accompanied by an exothermic oxidation reaction, when the ratio between citric acid (fuel) and oxidizer (metal nitrates) increased. The excessive heat transfer would allow ease rupture of the chemical bond in the gel precursor.

Acknowledgment

The authors thank the National Science Council of the Republic of China (Grant NSC 93-2113-M-014-001). Authors wish to express their gratitude to Miss S.Y. Lee and Miss J.C. Chen of NSC Instrument Center for XRD and EPR analysis.

References

[1] J.B. da Silva, N.D.S. Mohallem, J. Magn. Magn. Mater. 226–230 (2001) 1393.
[2] J. Plocek, A. Hutlova, D. Niznansky, J. Bursik, J.L. Rehspringer, Z. Micka, J. Non-Cryst. Solids 315 (2003) 70.
[3] C. Caizer, M. Popovici, C. Savii, Acta Mater. 51 (2003) 3607.
[4] J.H. Paterson, R. Devine, A.D.R. Phelps, J. Magn. Magn. Mater. 196–197 (1999) 394.
[5] T. Tsutaoka, T. Kasagi, K. Hatakeyama, J. Eur. Ceram. Soc. 19 (1999) 1531.
[6] E.M. Mohammed, K.A. Malini, P. Kurian, M.R. Anantharaman, Mater. Res. Bull. 37 (2002) 753.
[7] D.R. Sharma, R. Mathur, S.R. Vadera, N. Kumar, T.R.N. Kutty, J. Alloy. Compd. 358 (2003) 193.
[8] N.E. Kazantseva, J. Vilcakova, V. Krresalek, P. Saha, I. Sapurina, J. Stejskal, J. Magn. Magn. Mater. 269 (2004) 30.
[9] H.Y. Luo, Z.X. Yue, J. Zhou, J. Magn. Magn. Mater. 210 (2000) 104.
[10] L. Zhang, G.C. Papaefthymiou, R.F. Ziolo, J.Y. Ying, Nanostruct. Mater. 9 (1997) 185.
[11] N.D.S. Mohallem, L.M. Seara, Appl. Surf. Sci. 214 (2003) 143.
[12] D. Ravinder, K.V. Kumar, Mater. Lett. 49 (2001) 57.
[13] G.S. Li, L.P. Li, R.L. Smith Jr., H. Inomata, J. Mol. Struct. 560 (2001) 87.
[14] V.M. Bujoreamu, E. Segal, Solid State Sci. 3 (2001) 407.
[15] Z. Yue, J. Zhou, L. Li, X. Wang, Z. Gui, Mater. Sci. Eng. B 86 (2001) 64.
[16] J.H. Lee, C.K. Kim, S. Katoh, R. Murakami, J. Alloy. Compd. 325 (2001) 276.
[17] A. Chatterjee, D.D.D. Chakravorty, K. Choudhury, Appl. Phys. Lett. 57 (1990) 1360.
[18] Z. Yue, J. Zhou, L. Li, H. Zhang, Z. Gui, J. Magn. Magn. Mater. 208 (2000) 55.
[19] S.K. Saha, P. Pramanik, Br. Ceram. Trans. 96 (1997) 21.
[20] Z. Yue, L. Li, J. Zhou, H. Zhang, Z. Gui, Mater. Sci. Eng. B 64 (1999) 68.
[21] G. Ting-Kuo Fey, R.F. Shiu, V. Subramanian, C.L. Chen, Solid State Ionics 148 (2002) 291.
[22] K.H. Wu, Y.C. Chang, G.P. Wang, J. Magn. Magn. Mater. 269 (2004) 150.
[23] H.H.E. Kissinger, Anal. Chem. 29 (1957) 1702.
[24] D.W. van Krevelen, C. van Herden, F.J. Huntjens, Fuel 30 (1951) 253.
[25] R.D. Purohit, B.P. Sharma, K.T. Pillia, A.K. Tyagi, Mater. Res. Bull. 36 (2001) 2711.
[26] H.P. Klug, L.E. Alexander, X-ray Diffraction Procedures for Polycrystalline and Amorphous Materials, Wiley, New York, NY, 1997, p. 637.
[27] X. Li, G. Lu, S. Li, J. Alloy. Compd. 235 (1996) 150.
[28] J.F. Rabek, Experimental Methods in Polymer Chemistry—Physical Principles and Applications, Wiley, New York, 1980, p. 332.
[29] S. Liu, X. Tan, K. Li, R. Hughes, Ceram. Int. 28 (2002) 327.
[30] El-H.M. Diefallah, M.A. Mousa, A.A. El-Bellihi, E.H. El-Mossalamy, G.A. El-Sayed, M.A. Gabal, J. Anal. Appl. Pyrolysis 62 (2002) 205.